



Multi-temporal assessment of land surface temperatures as an indicator of land use/cover changes and climate variability in the Develi Basin, Turkey

Ali Muslim Amiri¹ · Filiz Dadaser-Celik¹

Received: 2 May 2022 / Accepted: 15 May 2023 / Published online: 24 May 2023

© The Author(s), under exclusive licence to Springer-Verlag GmbH Germany, part of Springer Nature 2023

Abstract

Land surface temperature (LST) is an important parameter that reflects land surface processes of water and energy balance and has been used in assessment of land use/cover changes. However, the use of LST in monitoring changes in non-urban areas such as agricultural areas and wetlands is still limited. In this study, we aim to determine the spatial and temporal changes in LST in a semi-arid agricultural basin in Turkey (Develi Basin), where land use/cover and climatic conditions showed considerable variability since 1980s. Irrigated agriculture have expanded in the basin since 1987, after the construction of a large irrigation project. The basin hosts an internationally important wetland, called the Sultan Marshes, affected negatively by irrigation expansion. The study covers a 39-year period from 1984 to 2022. Four Landsat Thematic Mapper (TM) images acquired in 1984, 1987, 2003, and 2007 and two Landsat 8 OLI/TIRS images acquired in 2014 and 2022 were used in the analyses. The land use/cover changes were evaluated based on Normalized Difference Vegetation Index (NDVI). LST was estimated through top-of-atmosphere brightness temperature from thermal bands of Landsat images. Climate variability from 2014 to 2022 was analyzed with statistical methods. The results indicated that Develi Basin faced both spatial and temporal land use/cover changes. The area covered with natural steppe vegetation and water bodies decreased in the basin. In contrast, the sparsely and densely vegetated soil covers, which mostly denote agricultural areas, increased. Changes in LST values were observed from 1984 to 2022 as a result of climatic factors and land use/cover changes. LST changes were variable across different land use/cover types; LST decreased in irrigated areas and increased in lakes that went dry over years. LST changes proved useful for evaluating land use/cover changes and climatic variations in agricultural basins.

Keywords Land surface temperature · Irrigated agriculture · Land use/cover · Normalized Difference Vegetation Index · Climate variability · Semi-arid

Introduction

Land surface temperature (LST) reflects land surface processes of water and energy balance (Zhang et al. 2022). The use of LST in environmental studies goes back to 1970s (Li et al. 2013). Many previous studies used LST to monitor land use/cover changes and particularly urban sprawl from regional to continental scales (Morabito et al. 2016; Nega and Balew 2022; Peng et al. 2018;

Stathopoulou and Cartalis 2007). LST shows sensitivity to expansion of impervious surfaces and has also been used as a tool for understanding urban heat island effect (Weng et al. 2004). Some other studies used LST for modelling the climatic system and surface energy balance (Bateni et al. 2013), estimation of evapotranspiration (Hari et al. 2021; Xiong and Qiu 2011), soil moisture (Gallego-Elvira et al. 2016), and mapping air temperatures (Zeng et al. 2015). LST has also been used to obtain information about spatial and temporal variations in a region (Anderson et al. 2008; Orhan et al. 2014; Ottlé et al. 2004). Although LST has been used in a variety of applications in several disciplines, the use of LST in monitoring land use/cover changes in non-urban areas such as agricultural areas and wetlands is still limited (Nega and Balew 2022). In this study, we aim to fill in this gap by studying how LST

Responsible Editor: Philippe Garrigues

✉ Filiz Dadaser-Celik
fdadaser@erciyes.edu.tr

¹ Department of Environmental Engineering, Erciyes University, Kayseri, Turkey

responded to land use/cover changes and climate variability in an agricultural basin that hosts a large wetland complex.

Agriculture and irrigation are among the most pervasive anthropogenic activities. Irrigated agriculture can alter hydrologic cycle, transform land use/cover, and even cause social-economic transformation and climate changes (Merchán et al. 2013; Mwakalila 2006). The impact of irrigated agriculture on LST received attention only in recent years. Yang et al. (2020a) examined LST changes across China using satellite remote sensing techniques and showed that irrigation can on average cause 1.5°C change in day-time land surface temperatures. By comparing the LST differences between irrigated areas and adjacent nonirrigated areas, Yang et al. (2020b) showed that all irrigated areas were cooler than nonirrigated areas across the globe. The magnitude of difference was $0.96 \pm 1.66^{\circ}\text{C}$ during daytime and $0.34 \pm 0.71^{\circ}\text{C}$ during nighttime. Liu et al. (2019) examined the LST changes in irrigated paddy fields in semi-arid western Jilin province of China and showed that the shift in land use to irrigated paddy fields caused significant decline in the LSTs. They further revealed that the LST changes in humid areas were minor, while they can be over 6°C in semi-arid regions. Not only the climatic setting but also the characteristics of the agricultural activities were important determinants of LST changes. A recent study showed that conversion from marshland to paddy field and dry farmland in China had different effects on LST (Shen et al. 2020).

These studies showed that LST parameter is highly sensitive to the land use/cover changes due to irrigated agriculture and therefore has the potential to provide new insights into our understanding of the effect of agricultural expansion and irrigation on the land surface. As can be seen from the literature review, the majority of the previous studies were conducted at large spatial scales, and LST changes were found to be more prominent in semi-arid regions. Local-level studies in semi-arid regions are needed to better understand the LST differences due to conversions among different land use/cover classes.

In this study, our objective is to examine LST changes in response to expansion of irrigated agriculture in a semi-arid basin (Develi Basin) in Turkey. Being an agricultural basin and hosting a very large wetland complex, Develi Basin provides a complex terrain to understand the relationships of land use/cover and LST changes. Our analyses examine how irrigation-induced changes affected LST over the basin. By analyzing a multi-temporal dataset, we also analyzed how the LST response to land use/cover changes differs under changing climatic conditions.

Materials and methods

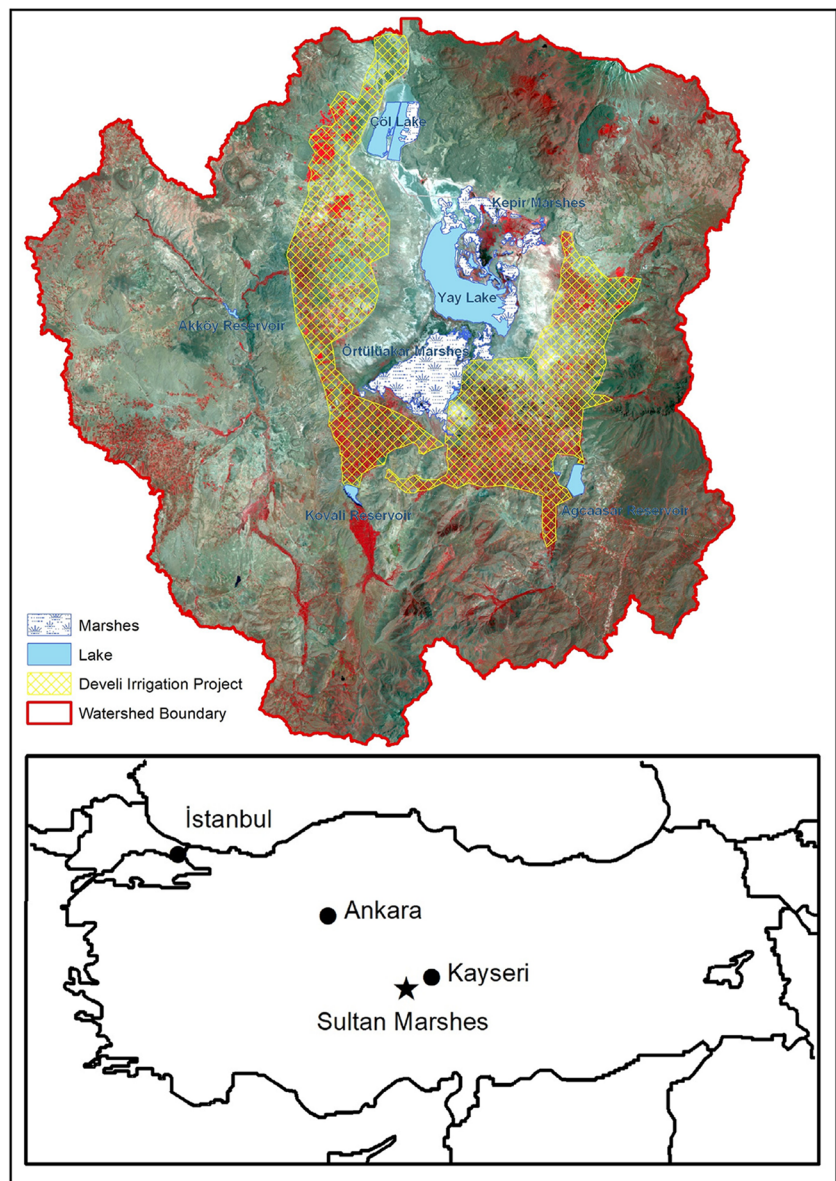
Study area

Develi Basin is a closed, semi-arid basin, located in the Central Anatolia Region of Turkey, southwest of the city of Kayseri (Fig. 1). The basin has an area of 800 km^2 and a drainage area of 3190 km^2 (DSI 1995). The Develi Basin's altitude is in the range of 1070–3916 m with an average of 1100 m. The main towns are Develi, Yahyalı, and Yeşilhisar, and the basin hosts a population of about 140,000.

An important aspect of Develi Basin is that wetlands constitute significant portion of the basin. The Sultan Marshes is a large wetland complex located at the center of the basin (Fig. 1). The marshes consist of four interconnected water systems. Yay Lake and Çöl Lake are shallow and saline lakes. There are two freshwater marshes, Örtülüakar and Kepir Marshes. The presence of saline and freshwater ecosystems provides habitat for a variety of species including over 300 species of birds (Karadeniz 2000). Despite the marshes are under protection as a Ramsar Site and National Park, they have been affected significantly by agricultural development in the last three decades recently (Dadaser-Celik et al. 2006, 2007, 2008a, b; Jouma and Dadaser-Celik 2017). The marshes and surrounding salt steppes and wet meadows covered almost 10% of the basin, but their area has shrunk through years, and even they went completely dry in some years (Dadaser-Celik et al. 2006; Jouma and Dadaser-Celik 2021).

Agriculture is the main economic activity in the Develi Basin, where about 60% is used for irrigated or nonirrigated farming. Three reservoirs (Kovalı, Ağcaasar, and Akköy) are located in the basin and used for flood irrigation (Fig. 1). Groundwater is used also extensively, when possible. Develi Irrigation Project, planned and constructed in 1980s, has changed the nature of agriculture in the basin. Before the completion of the project, only a small area (926 ha) was under irrigation by flows collected at Akköy Reservoir, constructed in 1967. For the rest of the basin, irrigation was only possible by a number of groundwater pumping facilities and/or at farmlands located along small streams. The construction of Kovalı and Ağcaasar Reservoirs and some other groundwater pumping facilities was completed in 1987, which made possible the irrigation of 28,000 ha of farmland. Since 1987, three irrigation reservoirs have been accumulating almost all surface flows, and irrigated agriculture with high-water consuming crop varieties has become more widespread in the basin (Dadaser-Celik et al. 2008b; Jouma and Dadaser-Celik 2021).

Fig. 1 Location and hydrologic features of the Develi Basin



Data used

In this study, we used climate data obtained from the Turkish State Meteorology Service and satellite imagery data obtained from the US Geological Survey (USGS).

The climate data included precipitation and air temperature data collected at the Develi Meteorology Station at the Develi province located to the southeast of the basin. Develi Meteorology Station was the only station that provided continuous data for the 1984 to 2022 period.

The satellite imagery data included Landsat data, which were preprocessed by NASA through atmospheric correction algorithms and radiometric calibration (level-1 products <http://earthexplorer.usgs.gov/>) and were freely accessible. The images were selected from the Landsat

achieve. Four criteria were applied during image acquisition. First, we preferred to select Landsat Thematic Mapper (TM), Landsat Enhanced Thematic Matter Plus (ETM+), or Landsat 8 Operational Land Imager/Thermal Infrared Sensor (OLI/TIRS) imagery, as they have comparable spatial and spectral resolutions. Landsat images are also available since 1980s, which provided opportunity for long-term analysis. Second, we preferred to obtain imagery for the late spring/early summer period, as this period provides the best distinction between irrigated and nonirrigated areas and can be referred as the best time interval for wetland observation (Dadaser-Celik et al. 2008b; Jouma and Dadaser-Celik 2021). Third, for the success of Normalized Difference Vegetation Index (NDVI) and LST calculations, cloud-free images were

selected. Finally, we preferred to obtain images, which were separated at certain time intervals. We searched the Landsat archive and tried to obtain best images that satisfy the four criteria. Unfortunately, the acquisition of imagery was challenging due to unavailability of cloud-free data during the time period selected. Therefore, our final dataset included four Landsat TM images acquired on 12 August 1984, 4 July 1987, 30 June 2003, and 11 July 2007 and two Landsat 8 OLI/TIRS images acquired on 14 July 2014 and 4 July 2022. The images were captured from 7:40 to 8:15 a.m. local time under clear atmospheric condition with the WRS2-package Path 175 Row 33 and Path 175 Row 34 location.

Climate data analysis

The climate dataset, consisting of daily air temperature and precipitation data series, covered the 1984–2022 period. The dataset was first checked for missing records. Both precipitation and air temperature time series were continuous except for a few days of missing records. All data were arranged as monthly/annual totals (precipitation) or averages (air temperature) before further analysis.

The trends in the climate data were analyzed to evaluate whether there is a monotonic upward or downward trend in air temperature and precipitation data series from 1984 to 2022. Although we see year-to-year variations or fluctuations in these data series, trend analysis can determine the general direction of changes and identify if these changes are statistically significant. For trend analysis, we used the nonparametric Mann–Kendall trend test (Kendall 1975; Mann 1945), which is a method used frequently for testing trends in hydrometeorological data. The magnitude of trends was estimated by the Sen's slope method. Sen's slope (Sen 1968) is also a nonparametric method and can be used to estimate the actual slope of Mann–Kendall trend analysis. The statistical significance of trends was evaluated at the 0.01 level.

In addition to trend analysis, we compared the average annual and monthly air temperature and precipitation values for the years 1984, 1987, 2002, 2007, 2014, and 2022. With this comparison, we aimed to capture year-to-year fluctuations in climatic conditions.

Satellite data analysis

The analysis of satellite imagery data was accomplished in three steps. In the first step, data preprocessing was applied to correct geometric and radiometric errors. In the second step, NDVI was calculated to determine land use/cover changes. LST calculation was done at the third step.

Data preprocessing

For each year, two images from Path 175 Row 33 (UP) and Path 175 Row 34 (DOWN) were acquired to cover the basin area. The UP and DOWN images were first mosaicked, and the basin area was extracted. Geometric correction and radiometric correction were applied to remove distortions of images due to satellite (e.g., attitude deviation from nominal), sensor (e.g., jitters, view angle effects), and Earth (e.g., rotation, relief, curvature)-based factors (Anonymous 2002). Images were rectified and resampled using 50 ground control points and georeferenced to the WGS1984 Datum and Universal Transverse Mercator (UTM) zone 36N coordinate system. Ground control points are points on the ground with known coordinates that are easily identifiable on the imagery. In this study, 50 points consisted of road and irrigation/drainage canal intersections. The coordinates of these points were either collected in the field with a GPS device or obtained from Google Earth, if located in an inaccessible location.

Four Landsat TM images were captured under clear atmospheric conditions. We assumed uniform atmospheric conditions within the images, and no atmospheric correction was applied. On Landsat 8 OLI/TIRS images, atmospheric scattering was detected; therefore, Dark Object Subtraction method (Chavez 1988) was applied in ENVI 5.3 for correcting the additive haze component.

NDVI derivation

NDVI was used to investigate land use/cover changes over the Develi Basin. NDVI is derived from the surface reflectance in the red and near infrared (NIR) parts of the electromagnetic spectrum and demonstrate the amount of vegetation in a specific area (Knippling 1970). The red and NIR channels (bands 3 and 4, respectively) of the Landsat TM with red and NIR channels (bands 4 and 5, respectively) of the Landsat OLI were used to calculate NDVI in the study area.

To acquire NDVI, the first step was to convert digital numbers (DN) to spectral radiance. The conversion to spectral radiance is the primary step in putting image into a common radiometric scale from multiple platforms and sensors (Chander and Markham 2003). The digital numbers of band 3 and 4 of Landsat TM and band 4 and 5 of Landsat 8 were converted to spectral radiance using Eqs. 1–3 for Landsat 8 data or Eq. 4 for Landsat TM data (Anonymous 2002, 2016):

$$L_{\lambda} = G_{\text{rescale}} * Q_{\text{CAL}} + B_{\text{rescale}} \quad (1)$$

where

$$G_{\text{rescale}} = L_{\text{MAX}} - L_{\text{MIN}} / Q_{\text{CALMAX}} \quad (2)$$

$$B_{\text{rescale}} = LMIN_{\lambda} \quad (3)$$

In Eq. 1, G_{rescale} ($\text{Wm}^{-2}\text{sr}^{-1}\mu\text{m}^{-1}/\text{DN}$) and B_{rescale} ($\text{Wm}^{-2}\text{sr}^{-1}\mu\text{m}^{-1}$) are band-specific rescaling factors.

$$L_{\lambda} = ((LMAX_{\lambda} - LMIN_{\lambda}) / (Q_{\text{CALMAX}} - Q_{\text{CALMIN}})) * (Q_{\text{CAL}} - Q_{\text{CALMIN}}) + LMIN_{\lambda} \quad (4)$$

In Eqs. 1–4, L_{λ} is the spectral radiance at the sensor ($\text{Wm}^{-2}\text{sr}^{-1}\mu\text{m}^{-1}$); $LMIN_{\lambda}$ and $LMAX_{\lambda}$ are the spectral radiance that is scaled to Q_{CALMIN} and Q_{CALMAX} ($\text{Wm}^{-2}\text{sr}^{-1}\mu\text{m}^{-1}$), respectively. Q_{CAL} is the quantized calibrated pixel values in DN; Q_{CALMIN} and Q_{CALMAX} are the minimum and maximum quantized calibrated pixel values (corresponding to $LMIN_{\lambda}$ and $LMAX_{\lambda}$) in DN, respectively. The values in Eqs. 1 and 2 were taken from metadata of Landsat TM and Landsat OLI images (Chander and Markham 2003).

The obtained spectral radiance values from red and NIR channels were then converted to planetary reflectance using Eq. 5 (Anonymous 2002, 2016):

$$\rho_p = \pi L_{\lambda} d^2 / (ESUN_{\lambda} \cos\theta_s) \quad (5)$$

In Eq. 5, ρ_p is planetary reflectance (unitless), π is 3.14, L_{λ} (see above), d is the Earth–Sun distance in astronomical units, $ESUN_{\lambda}$ is the mean solar exo-atmospheric irradiance, and θ_s is the solar zenith angle (degrees). All values were obtained from images' metadata.

Finally, NDVI was calculated using the difference surface reflectance values of red and NIR channels over the sum of surface reflectance values of the red and NIR channels (Eq. 6). NDVI was produced from calibrated and geometrically registered images and scaled in byte range. The NDVI values varies in the range of -1 to $+1$, where near to $+1$ values indicate green vegetation and near to -1 values indicate non-vegetated areas such as snow and water (Eidenshink 1992).

$$\text{NDVI} = (\rho_{\text{nir}} - \rho_{\text{red}}) / (\rho_{\text{nir}} + \rho_{\text{red}}) \quad (6)$$

In Eq. 6, ρ_{nir} is the surface reflectance at NIR wavelength, and ρ_{red} is the surface reflectance at red wavelength.

NDVI values vary from -1 to $+1$, and positive NDVI values close to 1 demonstrate dense vegetation areas (Stathopoulou and Cartalis 2007). Develi Basin was classified into four land use/cover categories as water, soil, sparsely vegetated soil, and densely vegetated soil according to NDVI values for the years 1984, 1987, 2003, 2007, 2014, and 2022. Pixels with NDVI values less than 0 were classified as water. Pixels with NDVI values between 0 and 0.2 were classified as bare soil, which essentially refer to natural steppe vegetation cover, which consist of grasslands in spring but become dry in summer when the images were

acquired. Pixels with NDVI values between 0.2 and 0.5 were classified as sparsely vegetated soil, and those bigger than 0.5 were classified as densely vegetated soil.

LST derivation

For LST derivation, we used thermal bands (10.4–12.5 μm) of Landsat TM and the thermal bands (10.6–12.51 μm) provided by the Landsat 8 TIRS sensor.

The digital numbers of band 6 for the Landsat TM images (1984, 1987, 2003, 2007) were first converted to spectral radiance using Eq. 4. In addition, the digital numbers of band 10 and 11 for the Landsat 8 TIRS image (2014 and 2022) were also converted to spectral radiance using Eq. 1.

Spectral radiance values of band 6 of Landsat TM and band 10, 11 of Landsat 8 TIRS were then converted to at-satellite temperature using Eq. 7 (Artis and Carnahan 1982):

$$T_B = K_2 / (\ln(K_1 / L_{\lambda} + 1)) \quad (7)$$

In Eq. 7, T_B is radiant surface temperature (Kelvin), K_1 is calibration constant ($\text{Wm}^2\text{sr}^1\mu\text{m}^{-1}$), K_2 is calibration constant 2 (Kelvin), and L_{λ} is the spectral radiance at sensor ($\text{Wm}^{-2}\text{sr}^{-1}\mu\text{m}^{-1}$). The values were available at the images' metadata.

At-satellite temperature was calculated under a uniform emissivity assumption and was obtained in reference to a blackbody. A blackbody is the surface that absorbs all electromagnetic energy and neither reflects nor transmits energy, and it is an ideal radiator. On the other hand, real objects either transmit or reflect energy and are not ideal radiators (Artis and Carnahan 1982).

Emissivity is calculated by NDVI thresholds method (NDVI^{THM}) presented by Sobrino et al. (2004). Based on this method, surface emissivity is determined based on NDVI, when NDVI is between 0 and 0.2 (bare soil) and between 0.5 and 1 (densely vegetated soil) (Table 1). When NDVI is between 0.2 and 0.5, the emissivity is calculated as in Eq. 8.

$$\varepsilon = \varepsilon_v P_v + \varepsilon_s (1 - P_v) + d\varepsilon \quad (8)$$

In Eq. 8, ε is the emissivity of mixture, ε_v is the emissivity of the vegetation, and ε_s is the emissivity of the soil, and P_v is the vegetation proportion derived considering to Carlson and Ripley (1997). P_v can be calculated as in Eq. 9.

Table 1 Emissivity values with land use/cover classes (Stathopoulou and Cartalis 2007)

NDVI range	Emissivity	Classes
NDVI < 0	0.990	Water
0 > NDVI < 0.2	0.969	Bare soil
0.2 > NDVI < 0.5	0.977	Sparsely vegetated soil
NDVI > 0.5	0.980	Densely vegetated

$$P_v = \left[\frac{NDVI - NDVI_{min}}{NDVI_{max} - NDVI_{min}} \right]^2 \quad (9)$$

In Eq. 9, $NDVI_{min}$ is equal to 0.2, and $NDVI_{max}$ is equal to 0.5.

The term $d\varepsilon$ can be calculated as:

$$d\varepsilon = (1 - \varepsilon_s)(1 - P_v)F\varepsilon_v \quad (10)$$

In Eq. 10, F is the shape factor and concerning the geometrical structure of vegetation, and a constant value of 0.55 is taken.

Based on Eidenshink (1992), the NDVI values less than 0 were assumed to be water, and a typical value 0.990 for the emissivity was used. Other emissivity values were defined based on Stathopoulou and Cartalis (2007), considering the similarity of methodology acquiring NDVI, stated in Table 1.

Certain methods can be used for retrieving emissivity, but considering Dash et al. (2002), in the LST, error less than 1% in emissivity can rise an error from 0.3 to 0.7°C for a hot and humid atmosphere and cold and dry atmosphere, respectively, which is quite small. Many studies developed algorithms to derive LST from Landsat dataset, such as Mono-Window Algorithm (Qin et al. 2001) and the Radiative Transfer Equation (Sobrino et al. 2004), which requires additional input parameters like water vapor and at-surface temperature content of atmosphere, and these inputs were also not available for the study area. For this reason, the method below was used, with no additional input parameters.

The emissivity-corrected temperature can be calculated using Eq. 11 (Artis and Carnahan 1982):

$$LST = T_B / (1 + (\lambda T_B / \rho) \ln e) \quad (11)$$

In Eq. 11, LST is the land surface temperature (Kelvin), T_B is at-satellite temperature (kelvin), λ is the wavelength of emitted radiance (11.5 μm), ρ is $h \times c / \sigma$ (1.438×10^{-2} m K), h is Planck's constant (6.26×10^{-34} Js), c is the velocity of

light (2.998×10^8 m/s), σ is Stefan Boltzmann's constant (1.38×10^{-23} J K⁻⁴), and e is the calculated emissivity. Finally, LST is converted from Kelvin to Celsius (Eq. 12).

$$LST(^\circ\text{C}) = LST(\text{Kelvin}) - 273.15 \quad (12)$$

Results

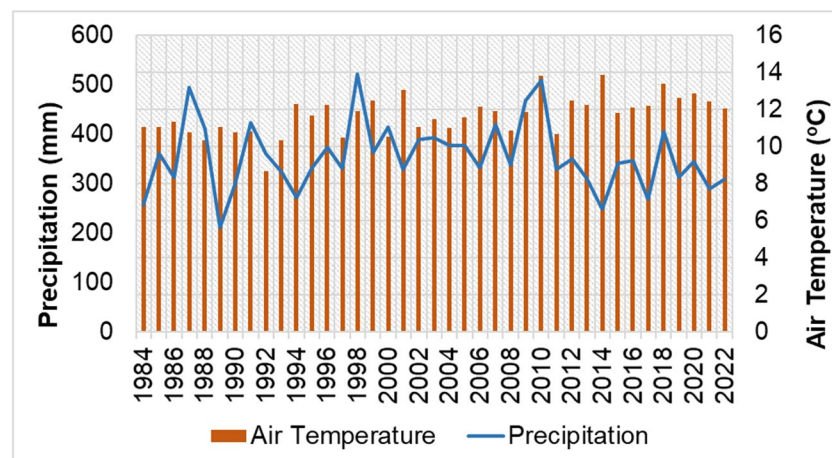
Climatic characteristics

Develi Basin has a continental climate with hot and dry summers and cold wet winters. The average annual air temperature was 11.7 °C (in the range of 8.7–13.8 °C) with maximum daily record of 38 °C and minimum daily record of –20 °C, and the average annual precipitation was about 354 mm (in the range of 210–520 mm) during the 1984–2022 period (Fig. 2).

The Mann–Kendall trend analysis showed that there is a statistically significant ($p < 0.01$) upward trend in air temperature data, and the trend magnitude was determined as 0.05 °C/year, corresponding to about 2 °C increase in air temperatures from 1984 to 2022. In contrast, the Mann–Kendall trend analysis detected no statistically significant trend in precipitation data at the 0.01 significance level. Although year-to-year fluctuations were present in precipitation data series, they did not create a monotonic upward or downward trend from 1984 to 2022.

Annual precipitation in years 1984, 1987, 2003, 2007, 2014, and 2022 were 256 mm, 495 mm, 392 mm, 419 mm, 248 mm, and 308 mm, respectively. Annual average temperature for the years 1984, 1987, 2003, 2007, 2014, and 2022 were 9.7 °C, 10 °C, 11 °C, 11 °C, 13.8 °C, and 12.1 °C, respectively (Fig. 2). Annual average temperatures in years 1984, 1987, 2003, 2007, 2014, and 2022 showed a consistent increase from 1984 to 2014. The year 2022 broke this rule,

Fig. 2 Annual average temperature (°C) and annual precipitation (mm) in the Develi Basin during the 1984–2022 period



having air temperature lower than the year 2014. The year 1984 was not only the coolest year, but also the year with the lowest annual precipitation, among the years selected for this study. 1987 was the wettest year and had also annual average temperature lower than those of 2003, 2007, 2014, and 2022.

Monthly air temperature for the months, at which the images were acquired, were 19.1 °C, 22.4 °C, 19.6 °C, 24.5 °C, 24.7 °C, and 21.7 °C for the years 1984, 1987, 2003, 2007, 2014, and 2022. Average monthly air temperature values showed a similar pattern with annual average temperature patterns, where we notice about 2 °C increase. For the same months, precipitation ranged between 0 and 10 mm in all years. This is an expected finding as the summers are almost always dry in the region.

Land use/cover characteristics

Over the entire study period, bare soil cover ($0 < \text{NDVI} < 0.2$), which denote natural cover consisting of bare lands or lands with very little vegetative cover, was the predominant land use/cover type, except for the year 2022, when the predominant land use/cover type was sparsely vegetated soil ($0.2 < \text{NDVI} < 0.5$). Bare soil covered the largest area in 1984 (73%). However, the areal coverage decreased through years and was only 23.1% in 2022. We also noticed that densely vegetated soil cover ($\text{NDVI} > 0.5$) showed an increase (3 to 13%) from 1984 to 2022. Sparsely vegetated soil covered the largest area in 2022 with 64.4%, while it covered 20% in 1984 (Table 2). The area covered with water ($\text{NDVI} < 0$) declined from 3% in 1984 to 0.1% in 2007 and 0.4% in 2022 in the basin. The area covered with water was comparatively higher in 1987, 1984, and 2014, respectively. In 2003, 2007, and 2022, water areas were almost lost. As can be seen on Fig. 3, Yay Lake, located in the center of the basin, become smaller from 1984 to 2022. Also we notice that new water bodies are formed after 1987 to the south of the basin. These water bodies are Kovalı and Ağcaşar Reservoirs constructed within the Develi Irrigation project.

The average NDVI values calculated for 1984, 1987, 2003, 2007, 2014, and 2022 varied between 0.21 and 0.26, while maximum NDVI varied from 0.79 to 0.91, and minimum NDVI varied from -0.92 to -0.52. The minimum NDVI for the years 1984, 1987, 2003, 2007, 2014, and 2022 were -0.92, -0.68, -0.53, -0.52, -0.72, and -0.83, respectively. The lowest minimum NDVI value was detected

in 1984, and the highest one was in 2007. The maximum NDVI values for the years 1984, 1987, 2003, 2007, 2014, and 2022 were 0.84, 0.79, 0.83, 0.84, 0.85, and 0.91, respectively. Maximum NDVI value was the highest in 2022 and the lowest in 1987.

Land surface temperature characteristics

Table 3 presents minimum, maximum, and average LST values for the years 1984, 1987, 2003, 2007, 2014, and 2022 for the Develi Basin. The average LST for the years 1984, 1987, 2003, 2007, 2014, and 2022 were 34.7 °C, 34.7 °C, 33.7 °C, 40.9 °C, 36.0 °C, and 31.4 °C, respectively (Fig. 4, Table 3). The average LST values varied between 31.4 and 40.9 °C, and the highest average LST was detected in 2007, and the lowest average LST was detected in 2022.

The maximum LST for all years varied from 46.3 to 58.0 °C. It was the highest in 2007 and the lowest in 1987. Minimum LST varied from 1.3 °C (1987) to 11.4 °C (2007).

Discussions

NDVI changes from 1984 to 2022

The analyses showed that bare soil class ($0 < \text{NDVI} < 0.2$), which denote areas with no or little vegetation cover, constituted the largest area in the Develi Basin in all years, except for 2022, when sparsely vegetated soil cover ($0.2 < \text{NDVI} < 0.5$) hold the largest area. This classification is consistent with land use/cover maps of the Develi Basin previously developed by Jouma and Dadaser-Celik (2021) for the years 1987, 1998, 2007, and 2013 based on the classification of Landsat images. In Jouma and Dadaser-Celik (2021)'s study, the land use/cover classes were different than those used in this study: grasslands/shrublands, croplands, permanent wetlands, water bodies, barren (dry lake basins), and urban/built-up. Grassland/shrublands covered the largest area, followed by croplands in all years. Based on the analysis of the 1987–2013 period, croplands were shown to constitute 20–34%, and grasslands/shrublands covered 74–64%. Densely vegetated soils class in our study corresponds to irrigated croplands or wetlands in Jouma and Dadaser-Celik (2021)'s study, while bare soil and sparsely vegetated soil in our study correspond to grasslands/shrublands or rainfed

Table 2 Percentage of area of water, soil, sparse vegetated soil, and densely vegetated soil in the Develi Basin, in 1984, 1987, 2003, 2007, 2014, and 2022

Land use/cover	1984 (%)	1987 (%)	2003 (%)	2007 (%)	2014 (%)	2022 (%)
Water bodies	3	2	0.2	0.1	1	0.4
Bare soil	73	50	50.4	60.4	48	23.1
Sparingly vegetated soil	20	45	45.4	33.5	42	64.4
Densely vegetated soil	4	3	4	6	9	13

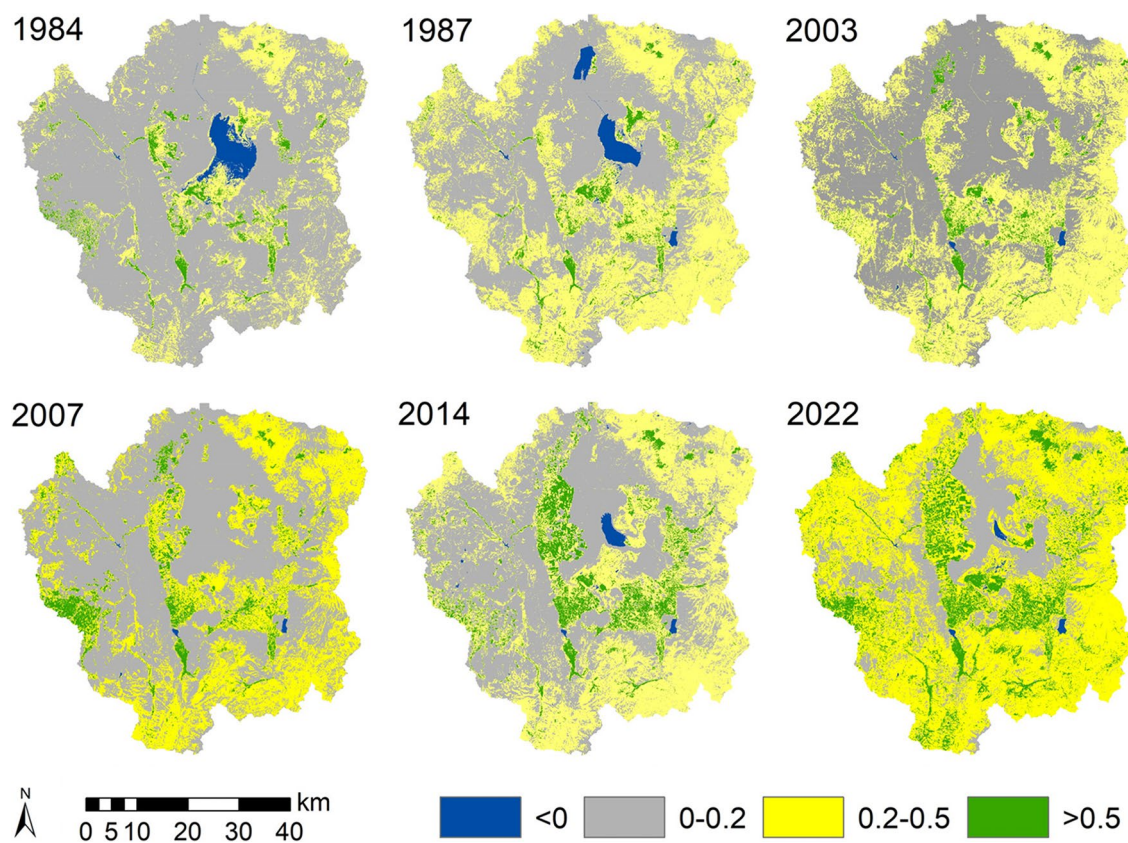


Fig. 3 NDVI values for the years 1984, 1987, 2003, 2007, 2014, and 2022 in the Develi Basin (<0=water, 0–0.2=bare soil, 0.2–0.5=sparingly vegetated soil, >0.5=densely vegetated soil)

Table 3 Minimum, maximum, and average LST (in °C) in the Develi Basin, in 1984, 1987, 2003, 2007, 2014, and 2022

Parameter	1984	1987	2003	2007	2014	2022
Minimum	8.9	1.3	4.5	11.4	1.6	7.5
Maximum	47.4	46.3	46.7	58.0	46.8	47.8
Average	34.7	34.7	33.7	40.9	36.0	31.4

croplands in the other. Although direct comparison is not possible, land use/cover changes documented in Jouma and Dadaser-Celik (2021) were also captured with NDVI analysis conducted in this study.

Based on the NDVI values, we see greenness increases from 1984 to 2022. The NDVI changes (Fig. 5, Fig. 6) between 1984 and 2022, determined by image subtraction method, clearly show that the vegetation increased in the majority of the basin from 1984 to 2022. The average value of NDVI change for the basin was 0.15, despite loss of marshlands, located at the center of the basin, which could have lowered NDVI values. In general, we see the transformation of bare soil cover to sparsely vegetated soil or densely vegetated soil and natural lakes and wetland areas converted to bare lands or sparsely vegetated areas. For a semi-arid basin such as Develi Basin, vegetation increase

during late spring/summer period could be either related to favorable climatic conditions or increase in irrigation practices. Our analysis showed that 2022 was a year, having about 2–3 °C higher air temperatures, compared to 1984. However, spring precipitation in 2022 was 120 mm, compared to 90 mm precipitation in spring of 1984. Higher spring precipitation could partially explain the increase in vegetation density in the basin. We notice that the NDVI increase was higher particularly in the agricultural areas irrigated within the Develi Irrigation Project (Fig. 6), pointing to the effect of irrigation activities on NDVI changes. Previous studies showed that irrigated agricultural areas have expanded in the region (Dadaser-Celik et al. 2006; Jouma and Dadaser-Celik 2021). Irrigated areas could easily be identified on Fig. 3 in the region covered by Develi Irrigation Project. Many previous studies also showed that

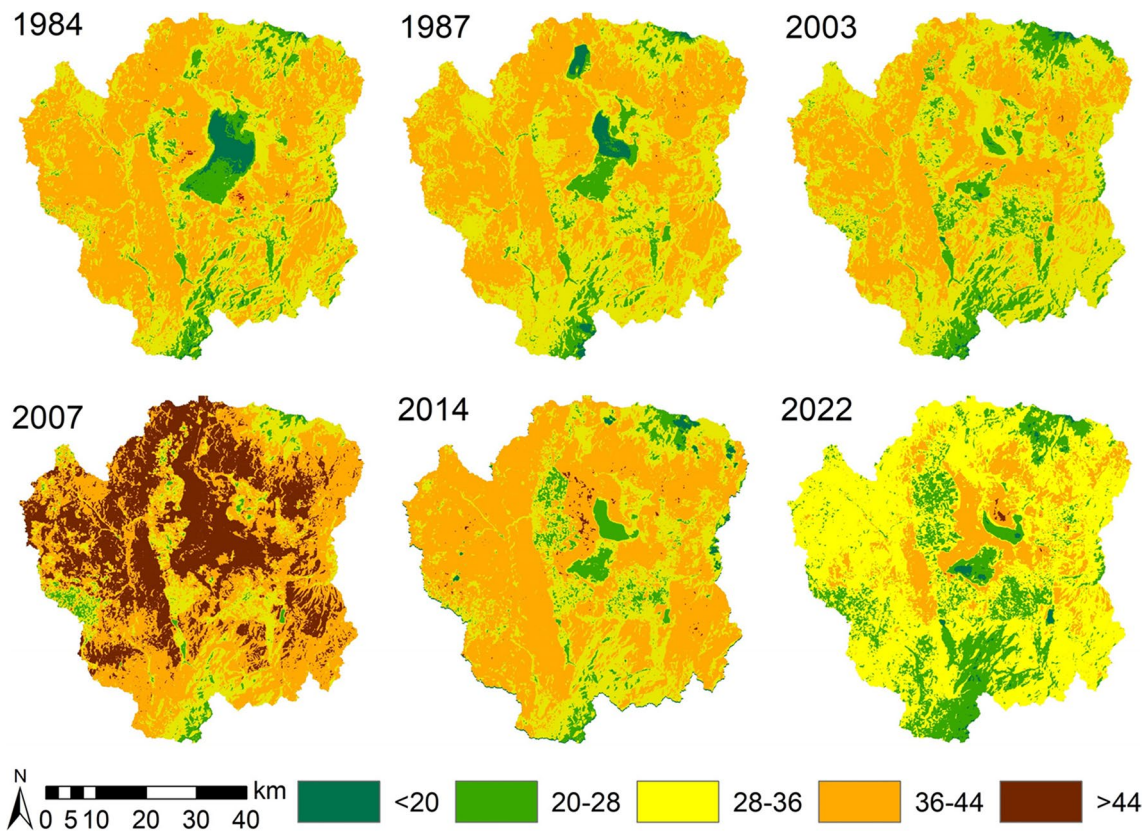
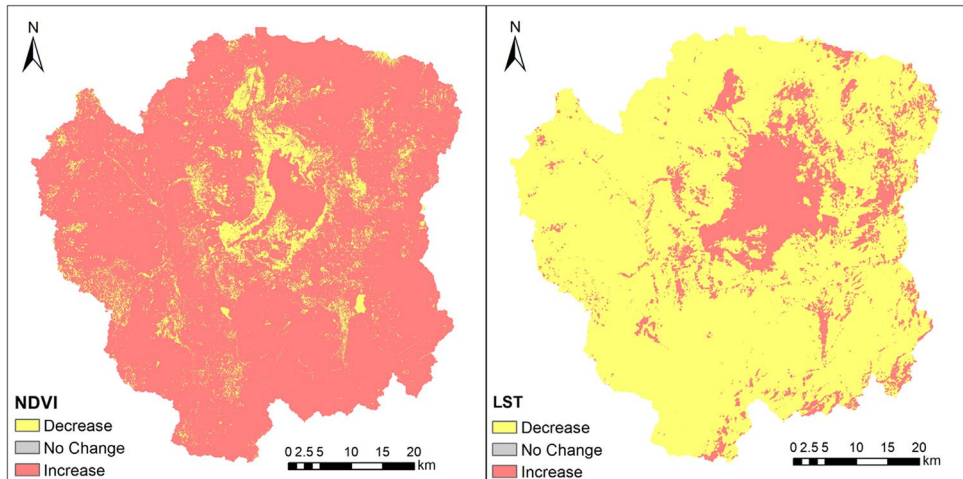


Fig. 4 LST values (in °C) for the years 1984, 1987, 2003, 2007, 2014, and 2022 in the Develi Basin

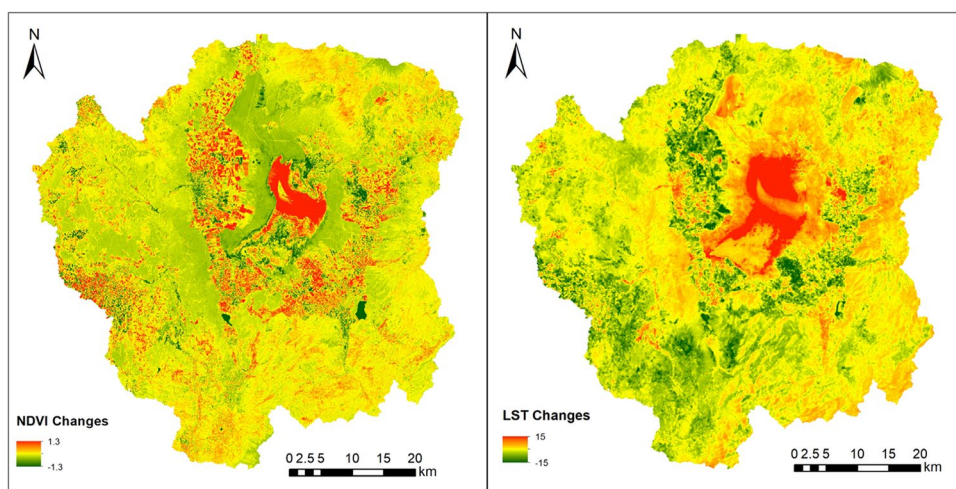
Fig. 5 The direction of NDVI and LST changes from 1984 to 2022



the expansion of irrigated agriculture creates significant changes in NDVI values. After analyzing trends in greenness in semi-arid regions over the world and their relationships with climatic variables, Fensholt et al. (2012) discussed that human disturbance (i.e., irrigation and fertilization) on the semi-arid regions could be an important factor on NDVI changes, and human disturbance can affect the relationship between climatic variables and NDVI. Fensholt

et al. (2012) also showed that increase in greenness in semi-arid areas in Central Turkey, where Develi Basin is located, could be explained by human influence rather than climatic variability. Zheng et al. (2019) analyzed NDVI changes in a semi-arid region in China and showed that climatic variations, land management practices that favor vegetation growth, and agricultural expansion were responsible for NDVI increases. Tian et al. (2020) discussed that irrigation

Fig. 6 The magnitude of NDVI and LST changes from 1984 to 2022



lessened drought impacts on agricultural lands and the NDVI of the irrigated lands changed larger than that of the nonirrigated lands in Australia. Xu et al. (2016) showed that the relationship between NDVI and climatic variables was stronger for grasslands than croplands due to moderating effect on irrigation on croplands.

Another factor that can cause an increase in average NDVI response in the Develi Basin is drying of lakes, particularly Yay Lake, located at the center of the basin. Dry lake basins were converted to either bare lands or sparsely vegetated soils. These areas, where $NDVI < 0$, declined from 3% in 1984 to 0.4% in 2022. Similar changes were previously documented for Develi Basin by Jouma and Dadaser-Celik (2021) and Dadaser-Celik et al. (2006, 2007) and for some other agricultural basins (Butt et al. 2015). Changes in lakes and wetlands in the Develi Basin were analyzed previously by many researchers, and climatic conditions as well as artificial factors such as changes in land use/cover and hydrology were found to be responsible for these changes (Dadaser-Celik et al. 2006, 2007; Jouma and Dadaser-Celik 2021, 2022).

The minimum and maximum NDVI showed small changes from 1984 to 2022. Extreme NDVI values can show the basin's response to large variations in climatic conditions, which may not be captured with the average NDVI values (Barbosa et al. 2006). Minimum NDVI value, which is related to the presence of water, was the lowest (-0.92) in 1984, where the water coverage was immense, and it was the highest in the year 2007 with a value of -0.52 , where the water coverage was the smallest. The minimum NDVI values were less than zero for all years. This could be due to water being in the form of snow at the higher elevations of the Mount Erciyes, located to the northwest of the basin (Yang et al. 2012). Maximum NDVI value, which is related to the presence of dense vegetation cover, was the highest in 2022.

LST changes from 1984 to 2022 and NDVI-LST relationships

The highest average LST for the basin was detected in 2007, and the lowest average LST was detected in 2022. When average LST values calculated for individual years were compared, the connections between LST values and general climatic conditions were found to be variable. For example, the year 2007 was the year with annual precipitation higher than that of 1984, 2003, 2014, and 2022. However, annual average temperature in 2007 was lower also than that of 2014 and 2022. We examined the direction and magnitude of LST changes by applying image subtraction between years 1984 and 2022. We found a decrease in average LST values for the entire basin at a value of about $3\text{ }^{\circ}\text{C}$ (Fig. 5, Fig. 6) from 1984 to 2022. This is again an interesting finding as air temperature in the basin showed an upward trend from 1984 to 2022, and the difference between annual average temperatures in 1984 and 2022 was about $2\text{ }^{\circ}\text{C}$. A similar difference in air temperatures was present on the monthly timescale: average monthly air temperature changed from 19.1 in 1984 to 21.7 in 2022.

We calculated correlation coefficients between average LST values and average annual air temperatures, average monthly air temperatures, and annual precipitation and found that the connection between LST and air temperatures was low at the annual timescale (with correlation coefficient of -0.04) but moderate at the monthly timescale (with correlation coefficient of 0.6). The correlation coefficient calculated between LST and annual precipitation was only 0.24 , pointing to much lower influence from precipitation changes. Due to the complexity of obtaining process of LST, a direct connection between LST and climatic variables is not always present (Yuan and Bauer 2007). Variations in land use/cover types, vegetation coverage, soil moisture, albedo, and roughness would affect land-atmosphere energy exchange processes and result in varied connections between air temperatures and LST

(Good et al. 2017; Xu et al. 2012). In this study, therefore, we studied the vegetation index, NDVI, as an indicator of changes in vegetation cover. There is strong correlation between NDVI and soil moisture (Zhang et al. 2018); therefore, NDVI analysis also provided the inclusion of soil moisture effects.

The LST values for different land use/cover types are presented in Table 4. In all years, LST was the lowest when NDVI is smaller than zero. For these areas, from 1984 to 2022, LST changed between 18 and 25 °C. These areas denote water-covered areas (i.e., lakes and reservoirs), which behave as heat sinks (Joshi and Bhatt 2012). Water-covered areas reduce the thermal effect of the ground and therefore have lower LST values compared to surrounding areas (Tan et al. 2020). Densely vegetated areas or areas with NDVI greater than 0.5 were the second coolest areas. These areas consist of marshes and wet meadows in the Sultan Marshes ecosystem and irrigated agricultural areas. LST, in these regions, ranged from 27 to 31 °C between 1984 and 2022. Marshes and wet meadows behave similar to water areas and have lower LST values (Tan et al. 2020). In these regions, vegetation and water acted as heat sinks (Joshi and Bhatt 2012). Deep-rooted vegetation respond much slowly to air temperature variations compared to bare soil areas and areas with shorter vegetation, as a result of the differences in aerodynamic and hydrological characteristics (Gallego-Elvira et al. 2016). The highest LST values were seen in bare soil areas where NDVI was between 0 and 0.2. In these regions, LST changed from 35 to 44 °C between 1984 and 2022. Due to the absence of vegetation cover, these areas do not reflect the energy as well and have much higher LSTs. Therefore, they respond much faster to air temperature variations (Gallego-Elvira et al. 2016).

Table 4 also explains why average LST values in 2022 were lower than that of 1984. In 2022, the dominant land use/cover class was sparsely vegetated soil with NDVI 0.2–0.5 and densely vegetated soil with NDVI > 0.5. These classes covered 77.4% of the basin. Average LST for these land use/cover types were 31 °C and 27 °C in 2022. In contrast, about 70% of the area was bare soil class in 1984, having average LST of 36 °C.

We examined the relationships of NDVI and LST values for all years (Fig. 7) to examine the relationships between land use/cover changes and LST. In general, an inverse correlation between LST and NDVI was detected when NDVI is

greater than zero, where low NDVI reveals high LST levels and high NDVI proposes low LST levels. Many previous studies showed that LST and NDVI values have negative relationships (Ghobadi et al. 2015; Yue et al. 2007). However, we notice that when NDVI is smaller than zero, there exists a slightly positive correlation between NDVI and LST. These areas denote lakes and reservoirs in the Develi Basin. Therefore, excluding pixels that correspond to lakes and reservoirs can make the correlation between NDVI and LST more stronger (Yue et al. 2007).

LST response in irrigated and nonirrigated areas

The results suggest that there is relationship between NDVI changes and LST values in the Develi Basin. Unfortunately, we do not have a database that show irrigated and nonirrigated agricultural areas clearly for the Develi Basin for different years. A detailed account of the types and sources of irrigation in the basin is not available. Previous studies showed that irrigation and crop selection decisions are made by farmers, and they change from year to year based on social and economic setting (Dadaser-Celik et al. 2008a, b). Also the irrigated parcels could change due to fallowing practices (Dadaser-Celik et al. 2008a, b).

However, based on previous studies, such as the land use/cover classification study conducted by Jouma and Dadaser-Celik (2021), we can assume that dense vegetation cover with NDVI > 0.5 located outside the marshlands in the Develi Basin are irrigated agricultural areas. We removed the Sultan Marshes wetland from the LST maps and calculated average LST for the areas where NDVI is greater than 0.5. The LST of these areas were not different than values reported in Table 4. Similar to the approach used in this study, some previous studies also used NDVI or land use/cover information to detect irrigated areas (Senturk et al. 2014; Wang et al. 2021) due to the difficulty of obtaining databases that show irrigated areas (Zohaib et al. 2019). Zhang et al. (2023) argued that the effect of irrigation on LST could be obtained by comparing LST of irrigated lands with those of other land use/cover classes.

For the 6 years analyzed in this study, we see that there is a 6–13 °C difference between LST of bare lands and densely vegetated soil areas and 3–6 °C difference between LST of sparsely vegetated soil and densely vegetated soil areas

Table 4 Average LST (in °C) of different land use/cover types in years 1984, 1987, 2003, 2007, 2014, and 2022

NDVI	LST	1984	1987	2003	2007	2014	2022
<0	18	20	22	25	24	21	
0–0.2	36	37	36	44	37	35	
0.2–0.5	32	34	32	38	33	31	
0.5–1	27	27	27	31	31	27	

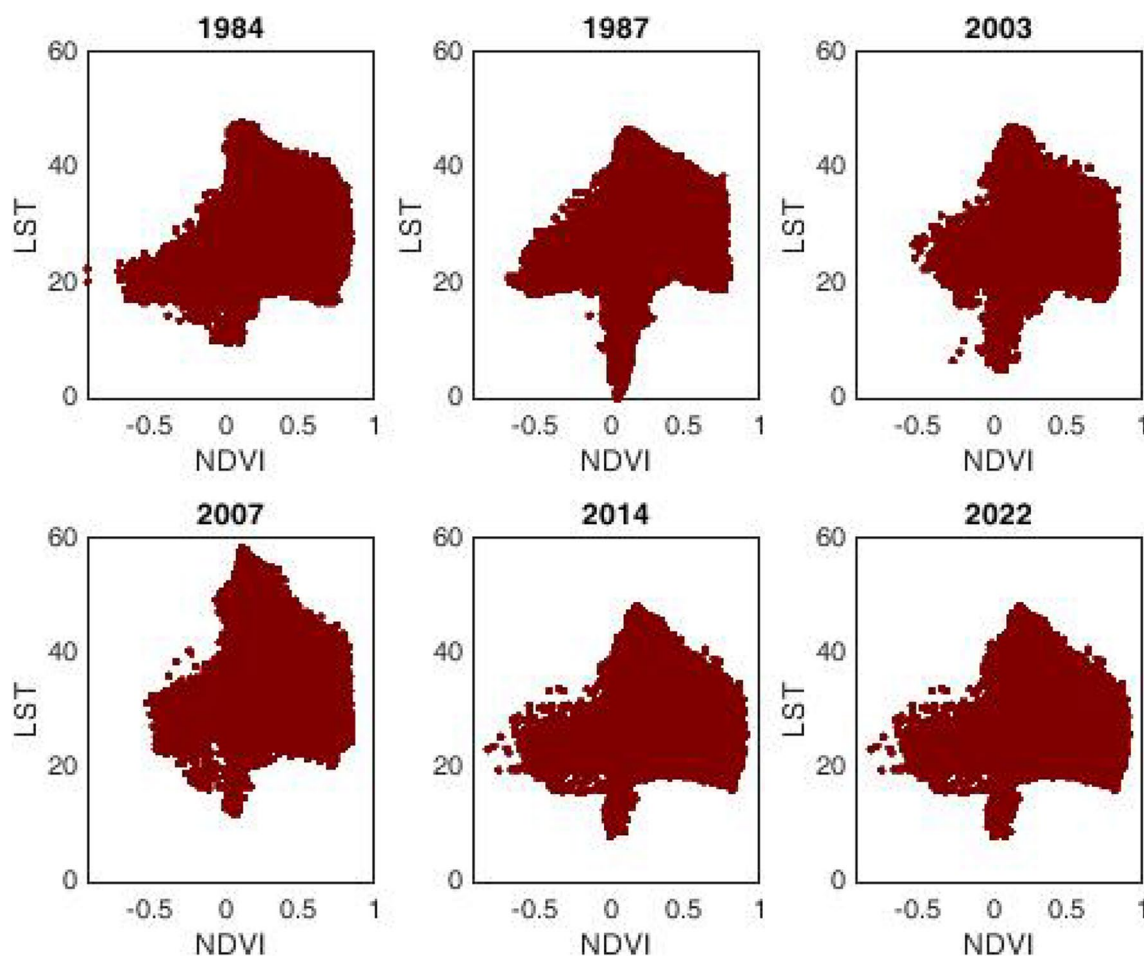


Fig. 7 Scatter plots of LST and NDVI in years 1984, 1987, 2003, 2007, 2014, and 2022

(Table 4). For all years, densely vegetated soil areas had LST values much lower than that of bare soil and sparsely vegetated soil areas. The difference between different classes is larger in 2007, the year with the highest average LST values and the lowest in 2014. Ambika and Mishra (2019) investigated the relationships between meteorological drought and vegetation stress in irrigated and nonirrigated areas in India and found that vegetation stress is reduced by irrigation. This can be the case for the Develi Basin as we see the largest NDVI and LST changes occurred in the areas irrigated within the Develi Irrigation Project (Fig. 7). Using a calibrated and evaluated Variable Infiltration Capacity model, Shah et al. (2019) argued that irrigation-caused cooling was more prominent in semi-arid climatic regions than subhumid ones. By using modelling studies, they further showed that mean annual LST lowers by 0.4 and 0.6 °C due to irrigation. Yang et al. (2020a) argued that irrigation-induced changes can be up to 6 °C in semi-arid regions. The results of this study were on the same order of magnitude with the LST differences determined in this study.

Limitations and future work

This study has some limitations, and further research can improve the results. LST changes determined in this study can be attributed to the combined effect of vegetation and climate changes. We argue that the increase in vegetation induced by irrigation played a major role on LST and moderated the LST increase that could have been possible due to air temperature increases. LST changes would have been different in the absence of irrigation and land use/cover changes. In this study, we were only able to analyze the relationship of NDVI and LST. Further research would be needed to understand the effects of other factors such as topography, soil moisture, soil types, and crop types on LST changes. Also in this study, we assumed that densely vegetated areas mostly covered irrigated agricultural areas. A correct account of irrigated and nonirrigated areas could put forward a clearer picture of irrigation influence on LST and can show the role of irrigation on NDVI and LST changes.

Conclusions

This study focused on the determination of LST and land use/cover changes based on remote sensing derived data in the Develi Basin, Turkey. The relationships between land use/cover, climatic conditions, and LST were analyzed for the region. The analysis covered a 39-year period from 1984 to 2022. NDVI analysis showed that there is an increase in vegetation cover/density in the Develi Basin during the study period. Water and bare soil areas decreased, while increases were detected in the areas covered by sparse and densely vegetated soils. The average change in NDVI was positive with a value of 0.15 from 1984 to 2022. LST analysis showed that LST decreased in the basin from 1984 to 2022, and the decrease was about 3 °C. For all years, average LST was the lowest for water class where NDVI is smaller than 0 and the highest for bare soil class where NDVI is between 0 and 0.2. A significant upward trend was detected in air temperatures in the region; therefore, LST decreases from 1984 to 2022 could be explained more with vegetation changes rather than climatic variability. We argued that irrigation moderated the LST increase that could have been possible due to air temperature increases. This study provided information about land use/cover and LST changes in the Develi Basin. The basin properties provided an opportunity to understand the effects of land use/cover transformation from natural steppe vegetation to irrigated agriculture. The results from this study can provide insights for land use/cover and LST changes in agricultural basins in semi-arid regions.

Author contribution Both authors contributed to the study design. Material preparation and data analysis were performed by Ali Muslim Amiri and Filiz Dadaser-Celik. The first draft of the manuscript was written by Ali Muslim Amiri. Filiz Dadaser-Celik prepared the final version. Both authors read and approved the final manuscript.

Funding This study was supported by the Scientific and Technological Research Council of Turkey (TUBITAK), Project Number: 114Y595 and the Research Fund of Erciyes University, Project Number: FYL-2018-7644.

Data availability The authors confirm that the data supporting the findings of this study are available within the article.

Declarations

Ethics approval and consent to participate Not applicable

Consent for publication All authors mutually agreed to publish the work in this journal.

Conflict of interest The authors declare no conflict of interests.

References

- Ambika AK, Mishra V (2019) Observational evidence of irrigation influence on vegetation health and land surface temperature in India. *Geophys Res Lett* 46:13441–13451
- Anderson MC, Norman JM, Kustas WP, Houborg R, Starks PJ, Agam N (2008) A thermal-based remote sensing technique for routine mapping of land-surface carbon, water and energy fluxes from field to regional scales. *Remote Sens Environ* 112:4227–4241
- Anonymous (2002) Landsat Project Science Office (2002) Landsat 7 science data user's handbook. Goddard Space Flight Center, NASA, Washington, DC
- Anonymous (2016) Landsat 8 data users handbook
- Artis DA, Carnahan WH (1982) Survey of emissivity variability in thermography of urban areas. *Remote Sens Environ* 12:313–329
- Barbosa HA, Huete AR, Baethgen WE (2006) A 20-year study of NDVI variability over the Northeast Region of Brazil. *J Arid Environ* 67:288–307
- Bateni SM, Entekhabi D, Jeng DS (2013) Variational assimilation of land surface temperature and the estimation of surface energy balance components. *J Hydrol* 481:143–156
- Butt A, Shabbir R, Ahmad SS, Aziz N (2015) Land use change mapping and analysis using remote sensing and GIS: a case study of Simly watershed, Islamabad, Pakistan. *The Egyptian Journal of Remote Sensing and Space Science* 18(2):251–259. <https://doi.org/10.1016/j.ejrs.2015.07.003>
- Carlson TN, Ripley DA (1997) On the relation between NDVI, fractional vegetation cover, and leaf area index. *Remote Sens Environ* 62:241–252
- Chander G, Markham B (2003) Revised Landsat-5 TM radiometric calibration procedures and postcalibration dynamic ranges. *IEEE Trans Geosci Remote Sens* 41:4
- Chavez PS (1988) An improved dark-object subtraction technique for atmospheric scattering correction of multispectral data. *Remote Sens Environ* 24:459–479
- Dadaser-Celik F, Stefan HG, Brezonik PL (2006) Dynamic hydrologic model of the Örtülüükar Marsh in Turkey. *Wetlands* 26:1089–1102
- Dadaser-Celik F, Bauer ME, Brezonik PL, Stefan HG (2008a) Changes in the sultan marshes ecosystem (Turkey) in satellite images 1980–2003. *Wetlands* 28:852–865
- Dadaser-Celik F, Brezonik PL, Stefan HG (2008b) Agricultural and environmental changes after irrigation management transfer in the Develi Basin, Turkey. *Irrig Drain Syst* 22:47–66
- Dadaser-Celik F, Brezonik PL, Stefan HG (2007) Hydrologic sustainability of the Sultan Marshes in Turkey. *Water International*
- Dash P, Götsche FM, Olesen FS, Fischer H (2002) Land surface temperature and emissivity estimation from passive sensor data: theory and practice-current trends. *Int J Remote Sens* 23:2563–2594
- DSI 1995 Develi-Yesilhisar Ovası Revize Hidrojeolojik Etüdu (Revised Hydrogeologic Study of Develi-Yesilhisar Basin), Devlet Su Isleri (State Hydraulic Works), Ankara, Turkey
- Eidenshink JC (1992) The 1990 conterminous U. S. AVHRR data set. *Photogramm Eng Remote Sens* 58:809–813
- Fensholt R, Langanke T, Rasmussen K, Reenberg A, Prince SD, Tucker C, Scholes RJ, Le QB, Bondeau A, Eastman R, Epstein H, Gaughan AE, Hellden U, Mbow C, Olsson L, Paruelo J, Schweitzer C, Sequist J, Wessels K (2012) Greenness in semi-arid areas across the globe 1981–2007 — an Earth Observing Satellite based analysis of trends and drivers. *Remote Sens Environ* 121:144–158

- Gallego-Elvira B, Taylor CM, Harris PP, Ghent D, Veal KL, Folwell SS (2016) Global observational diagnosis of soil moisture control on the land surface energy balance. *Geophys Res Lett* 43:2623–2631
- Ghobadi Y, Pradhan B, Shafri HZM, Kabiri K (2015) Assessment of spatial relationship between land surface temperature and land use/cover retrieval from multi-temporal remote sensing data in South Karkheh Sub-basin, Iran. *Arab J Geosci* 8:525–537
- Good EJ, Ghent DJ, Bulgin CE, Remedios JJ (2017) A spatiotemporal analysis of the relationship between near-surface air temperature and satellite land surface temperatures using 17 years of data from the ATSR series. *J Geophys Res Atmos* 122:9185–9210
- Hari M, Tyagi B, Huddar MSK, Harish A (2021) Satellite-based regional-scale evapotranspiration estimation mapping of the rice bowl of Tamil Nadu: a little water to spare*. *Irrig Drain* 70:958–975
- Joshi JP, Bhatt B (2012) Estimating temporal land surface temperature using remote sensing: a study of Vadodara urban area, Gujarat. *Int J Geol Earth Environ Sci* 2:123–130
- Jouma N, Dadaser-Celik F (2017) Spatiotemporal changes at the Sultan Marshes Ecosystem (Turkey) from 1987 to 2013. *Ecology* 2017, Kayseri, Turkey
- Jouma N, Dadaser-Celik F (2021) Landscape transformation after irrigation development in and around a semi-arid wetland ecosystem. *Landscape Ecol Eng* 17:439–457
- Jouma N, Dadaser-Celik F (2022) Assessing hydrologic alterations due to reservoirs and intensified irrigation in a semi-arid agricultural river basin using SWAT*. *Irrig Drain* 71:452–471
- Karadeniz N (2000) Sultan Sazligi, Ramsar site In Turkey. *Humedales Mediterraneos* 1:107–114
- Kendall M (1975) Rank correlation measures. Charles Griffin, London 202, 15
- Knippling EB (1970) Physical and physiological basis for the reflectance of visible and near-infrared radiation from vegetation. *Remote Sens Environ* 1:155–159
- Li Z-L, Tang B-H, Wu H, Ren H, Yan G, Wan Z, Trigo IF, Sobrino JA (2013) Satellite-derived land surface temperature: current status and perspectives. *Remote Sens Environ* 131:14–37
- Liu T, Yu L, Zhang S (2019) Land surface temperature response to irrigated paddy field expansion: a case study of semi-arid Western Jilin Province, China. *Sci Rep* 9:5278
- Mann HB (1945) Nonparametric tests against trend. *Econometrica: Journal of the Econometric Society* 13:245–259
- Merchán D, Causapé J, Abrahao R (2013) Impact of irrigation implementation on hydrology and water quality in a small agricultural basin in Spain. *Hydrol Sci J* 58:1400–1413
- Morabito M, Crisci A, Messeri A, Orlandini S, Raschi A, Maracchi G, Munafò M (2016) The impact of built-up surfaces on land surface temperatures in Italian urban areas. *Sci Total Environ* 551–552:317–326
- Mwakalila S (2006) Socio-economic impacts of irrigated agriculture in Mbarali District of south-west Tanzania. *Phys Chem Earth, Parts A/B/C* 31:876–884
- Nega W, Balew A (2022) The relationship between land use land cover and land surface temperature using remote sensing: systematic reviews of studies globally over the past 5 years. *Environ Sci Pollut Res* 29:42493–42508
- Orhan O, Ekercin S, Dadaser-Celik F (2014) Use of Landsat land surface temperature and vegetation indices for monitoring drought in the Salt Lake Basin Area, Turkey. *Sci World J* 2014:142939
- Ottlé C, Nerry F, Lagouarde JP, Kerr YH (2004) Land surface temperature retrieval techniques and applications: case of the AVHRR, thermal remote sensing in land surface processing. CRC Press, pp. 55–131
- Peng J, Ma J, Liu Q, Liu Y, Yn Hu, Li Y, Yue Y (2018) Spatial-temporal change of land surface temperature across 285 cities in China: an urban-rural contrast perspective. *Sci Total Environ* 635:487–497
- Qin Z, Karnieli A, Berliner P (2001) A mono-window algorithm for retrieving land surface temperature from Landsat TM data and its application to the Israel-Egypt border region. *Int J Remote Sens* 22:3719–3746
- Sen PK (1968) Estimates of the regression coefficient based on Kendall's tau. *J Am Stat Assoc* 63:1379–1389
- Senturk S, Bagis S, Ustundag BB (2014) Application of remote sensing techniques in locating dry and irrigated farmland parcels, 2014 The Third International Conference on Agro-Geoinformatics, pp. 1–4
- Shah HL, Zhou T, Huang M, Mishra V (2019) Strong influence of irrigation on water budget and land surface temperature in Indian Subcontinental River Basins. *J Geophys Res Atmos* 124:1449–1462
- Shen X, Liu B, Jiang M, Lu X (2020) Marshland loss warms local land surface temperature in China. *Geophys Res Lett* 47:e2020GL087648
- Sobrino JA, Jiménez-Muñoz JC, Paolini L (2004) Land surface temperature retrieval from LANDSAT TM 5. *Remote Sens Environ* 90:434–440
- Stathopoulou M, Cartalis C (2007) Daytime urban heat islands from Landsat ETM+ and Corine land cover data: an application to major cities in Greece. *Sol Energy* 81:358–368
- Tan J, Yu D, Li Q, Tan X, Zhou W (2020) Spatial relationship between land-use/land-cover change and land surface temperature in the Dongting Lake area, China. *Sci Rep* 10:9245
- Tian F, Wu J, Liu L, Leng S, Yang J, Zhao W, Shen Q (2020) Exceptional drought across Southeastern Australia caused by extreme lack of precipitation and its impacts on NDVI and SIF in 2018. *Remote Sens* 12:54
- Wang Z, Vivoni ER, Bohn TJ, Wang Z-H (2021) A multiyear assessment of irrigation cooling capacity in agricultural and urban settings of Central Arizona. *JAWRA J Am Water Resour Assoc* 57:771–788
- Weng Q, Lu D, Schubring J (2004) Estimation of land surface temperature–vegetation abundance relationship for urban heat island studies. *Remote Sens Environ* 89:467–483
- Xiong YJ, Qiu GY (2011) Estimation of evapotranspiration using remotely sensed land surface temperature and the revised three-temperature model. *Int J Remote Sens* 32(20):5853–5874. <https://doi.org/10.1080/01431161.2010.507791>
- Xu Y, Qin Z, Shen Y (2012) Study on the estimation of near-surface air temperature from MODIS data by statistical methods. *Int J Remote Sens* 33:7629–7643
- Xu Y, Yang J, Chen Y (2016) NDVI-based vegetation responses to climate change in an arid area of China. *Theoret Appl Climatol* 126:213–222
- Yang Y, Xu J, Hong Y, Lv G (2012) The dynamic of vegetation coverage and its response to climate factors in Inner Mongolia, China. *Stoch Env Res Risk Assess* 26:357–373
- Yang Q, Huang X, Tang Q (2020a) Irrigation cooling effect on land surface temperature across China based on satellite observations. *Sci Total Environ* 705:135984
- Yang Q, Huang X, Tang Q (2020b) Global assessment of the impact of irrigation on land surface temperature. *Sci Bull* 65:1440–1443
- Yuan F, Bauer ME (2007) Comparison of impervious surface area and normalized difference vegetation index as indicators of surface urban heat island effects in Landsat imagery. *Remote Sens Environ* 106:375–386
- Yue W, Xu J, Tan W, Xu L (2007) The relationship between land surface temperature and NDVI with remote sensing:

- application to Shanghai Landsat 7 ETM+ data. *Int J Remote Sens* 28:3205–3226
- Zeng L, Wardlow BD, Tadesse T, Shan J, Hayes MJ, Li D, Xiang D (2015) Estimation of daily air temperature based on MODIS land surface temperature products over the Corn Belt in the US. *Remote Sens* 7
- Zhang H, Chang J, Zhang L, Wang Y, Li Y, Wang X (2018) NDVI dynamic changes and their relationship with meteorological factors and soil moisture. *Environ Earth Sci* 77:582
- Zhang T, Zhou Y, Zhu Z, Li X, Asrar GR (2022) A global seamless 1km resolution daily land surface temperature dataset (2003–2020). *Earth Syst Sci Data* 14:651–664
- Zhang C, Ge Q, Dong J, Zhang X, Li Y, Han S (2023) Characterizing spatial, diurnal, and seasonal patterns of agricultural irrigation expansion-induced cooling in Northwest China from 2000 to 2020. *Agric Meteorol* 330:109304
- Zheng K, Ye J-S, Jin B-C, Zhang F, Wei J-Z, Li F-M (2019) Effects of agriculture, climate, and policy on NDVI change in a semi-arid river basin of the Chinese Loess Plateau. *Arid Land Res Manag* 33:321–338
- Zohaib M, Kim H, Choi M (2019) Detecting global irrigated areas by using satellite and reanalysis products. *Sci Total Environ* 677:679–691

Publisher's note Springer Nature remains neutral with regard to jurisdictional claims in published maps and institutional affiliations.

Springer Nature or its licensor (e.g. a society or other partner) holds exclusive rights to this article under a publishing agreement with the author(s) or other rightsholder(s); author self-archiving of the accepted manuscript version of this article is solely governed by the terms of such publishing agreement and applicable law.